

DOE/ID/12079--42

DE82 019949

Self-Potential Modeling from Primary Flows

William R. Sill

Department of Geology and Geophysics

University of Utah

Salt Lake City, Utah

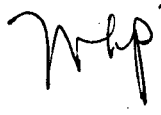
March 1981

Work performed under contract number DE-AC07-⁷⁹80ID12079
for Department of Energy, Division of Geothermal Energy

DISCLAIMER

This report was prepared as an account of work sponsored by an agency of the United States Government. Neither the United States Government nor any agency thereof, nor any of their employees, makes any warranty, express or implied, or assumes any legal liability or responsibility for the accuracy, completeness, or usefulness of any information, apparatus, product, or process disclosed, or represents that its use would not infringe privately owned rights. Reference herein to any specific commercial product, process, or service by trade name, trademark, manufacturer, or otherwise, does not necessarily constitute or imply its endorsement, recommendation, or favoring by the United States Government or any agency thereof. The views and opinions of authors expressed herein do not necessarily state or reflect those of the United States Government or any agency thereof.

DISTRIBUTION OF THIS DOCUMENT IS UNLIMITED



DISCLAIMER

This report was prepared as an account of work sponsored by an agency of the United States Government. Neither the United States Government nor any agency Thereof, nor any of their employees, makes any warranty, express or implied, or assumes any legal liability or responsibility for the accuracy, completeness, or usefulness of any information, apparatus, product, or process disclosed, or represents that its use would not infringe privately owned rights. Reference herein to any specific commercial product, process, or service by trade name, trademark, manufacturer, or otherwise does not necessarily constitute or imply its endorsement, recommendation, or favoring by the United States Government or any agency thereof. The views and opinions of authors expressed herein do not necessarily state or reflect those of the United States Government or any agency thereof.

DISCLAIMER

Portions of this document may be illegible in electronic image products. Images are produced from the best available original document.

NOTICE

This report was prepared to document work sponsored by the United States Government. Neither the United States nor its agent, the United States Department of Energy, nor any Federal employees, nor any of their contractors, subcontractors or their employees, makes any warranty, express or implied, or assumes any legal liability or responsibility for the accuracy, completeness, or usefulness of any information, apparatus, product or process disclosed, or represents that its use would not infringe privately owned rights.

NOTICE

Reference to a company or product name does not imply approval or recommendation of the product by the University of Utah or the U.S. Department of Energy to the exclusion of others that may be suitable.

CONTENTS

	PAGE
Abstract	1
Introduction	2
Coupled Flows	4
Numerical Modeling	9
Model Results	12
Field Example	19
Summary	21
Acknowledgements	22
References	23

ABSTRACT

A new method for the calculation of self potentials (SP) based on induced current sources is presented. The induced current sources are due to divergences of the convective current which is driven, in turn, by a primary flow, either heat or fluid. Numerical modeling utilizing this method has been implemented using a two-dimensional transmission surface algorithm. When the primary flow is driven by the gradient of a potential, joint modeling of the primary flow and the resultant SP is possible with this algorithm.

Examples of simple geometrical models in the presence of point sources for the primary flow are presented and discussed. Lastly, a field example of the joint modeling of temperature and SP data is illustrated with data from Red Hill Hot Spring, Utah.

INTRODUCTION

The self potential (SP) method is based on the measurement of naturally occurring potential differences generated mainly by electrochemical, electrokinetic and thermoelectric sources. The multiplicity of sources can be either an advantage or a disadvantage. On the one hand, a number of phenomena can be studied with the techniques and, on the other hand, the possibility of a number of different sources can sometimes be confusing.

There has been a mild resurgence in the use of the SP method in geothermal exploration (Corwin and Hoover, 1979), in the study of earthquake related phenomena (Fitterman, 1978; Corwin and Morrison, 1977), and in engineering applications (Ogilvy et al., 1969; Bogoslovsky and Ogilvy, 1973).

Older methods of interpretation were mostly based on polarized spheres (de Witte, 1948; Yungul, 1950) or line dipole current sources (Meiser, 1962; Paul, 1965). Although these techniques are useful, they provide little information about the nature of the primary sources. Nourbehecht (1963), drawing on the earlier work of Marshall and Madden (1959), discussed the source mechanisms in detail and provided a technique for the solution of coupled flows which incorporated the primary driving potential. His solution is formulated in terms of a total (pseudo) potential composed of the electric potential and the weighted primary source potential (pressure, temperature, concentration). In this formulation, the total (pseudo) potential depends only on the value of the primary

potential at the boundaries where there is a change in the coupling parameters, and its value inside the various media is immaterial. Unfortunately, this aspect of the total (pseudo) potential method has sometimes led to the neglect of the details of the primary flow, resulting in some calculations for inappropriate models as will be discussed in a subsequent section.

The purpose of this paper is to present an alternative method for the solution of coupled flow problems that explicitly models both the primary flow and the induced secondary electric potentials (joint modeling). The use of this technique with a two-dimensional (2-D) algorithm for potential problems provides a new flexibility in the modeling of SP data.

COUPLED FLOWS

The general equation for coupled flows can be written (Marshall and Madden, 1959; Nourbehecht, 1963)

$$\Gamma_i = \sum_j L_{ij} X_j, \quad (1)$$

where the fluxes Γ_i (charge, matter, heat, etc.) are related to the various forces X_j (gradients of electric potential, pressure, temperature, etc.) through the coupling coefficients ("conductivities") L_{ij} . For many practical applications of coupled flows, we are concerned with secondary electric current flows and potentials which are driven by some other primary flow. When the effects of the secondary electric potentials on the primary flow are small, the primary flow equation is decoupled and the resulting equations are

$$\Gamma_1 = -L_{11} \nabla \zeta, \quad (2)$$

$$\text{and } J_{\text{Total}} = \Gamma_2 = -L_{21} \nabla \zeta - \sigma \nabla \phi, \quad (3)$$

where Γ_1 is the primary flow (solution flux, heat flux, etc.), L_{11} is the primary conductivity (permeability, thermal conductivity, etc.) and ζ is the primary potential (pressure, temperature, etc.), J_{Total} is the total electric current, L_{21} is the cross coupling "conductivity", σ is the ordinary electrical conductivity and ϕ is the electric potential. The decoupled primary flow problem (equation 2) can be solved separately and used in the solution of the electrical flow problem (equation 3). As noted in the introduction, one

technique for the solution of equation 3 makes use of the total (pseudopotential) potential ψ , where $\psi = \phi + L_{21}\zeta / \sigma$. The technique used in this paper makes use of a different approach. Starting with equation 3, we note that the first term is a "convection" current driven by the primary flow and the second term is the usual conduction current driven by the gradient of the electric potential. Using this approach, we can write equation 3 as

$$J_{\text{Total}} = J_{\text{conv}} + J_{\text{cond}} \quad , \quad (4)$$

where $J_{\text{conv}} = -L_{21}\nabla\zeta$, (5)

and $J_{\text{cond}} = -\sigma\nabla\phi$. (6)

If no external current sources are imposed and we have DC conditions (i.e. $\partial\rho/\partial t = 0$), then the total current is divergenceless ($\nabla \cdot J_{\text{Total}} = 0$) and

$$\nabla \cdot J_{\text{cond}} = -\nabla \cdot J_{\text{conv}} = \nabla \cdot (L_{21}\nabla\zeta) = \nabla L_{21} \cdot \nabla\zeta + L_{21}\nabla^2\zeta. \quad (7)$$

Thus there are sources (non-zero divergence) of conduction current wherever there are gradients of the cross coupling coefficient parallel to the primary flow (flow perpendicular to boundaries) or wherever there are sources of the primary flow. The sources of the conduction current given by the right-hand side of equation 7 can then be used to determine the resultant electric potential, ϕ . There is also a similarity between equation 3 and the basic equations of magnetostatics and electrostatics in material media. For example, in the case of magnetostatics, J_{Total} is analogous to B (divergenceless), $-L_{21}\nabla\zeta$ takes the place of the induced magnetization M and $-\sigma\nabla\phi$ is

analogous to μH . Recall that in magnetostatics, $\nabla \cdot M$ gives rise to magnetic charge densities, just as in the coupled flow problem $\nabla \cdot (L_{21} \nabla \zeta)$ gives rise to current densities.

The use of this analogy is somewhat limited by the fact that in geophysical applications we deal with the boundary condition of zero normal component of the total current flow at the air-earth interface. The analogous boundary condition on normal B is not commonly used in magnetostatic problems. However, since many geophysicists are familiar with magnetostatics, this analogy should provide some intuitive feeling for the form of the induced electrical flows in coupling problems, if the slightly different boundary conditions are taken into account.

The use of equation 7 and the nature of the coupling coefficient can be demonstrated for the case of uniform primary flow perpendicular to plane boundaries (Figure 1). At $x = 0, h$, there are planes of current sources. Using the boundary conditions of no current flow in regions 1 and 3, the solution of this problem gives constant potentials in regions 1 and 3 and a linearly increasing potential in region 2. The constant electric field ($E = -\nabla \phi = L_{21} \nabla \zeta / \sigma$) in region 2 drives a current that exactly cancels the convection current ($L_{21} \nabla \zeta$) and the total current is zero everywhere.

This geometry of flow is similar to that used in typical laboratory measurements of coupling coefficients. For example, if the gradients of primary and electric potential (or the potential drops) are measured under the conditions of zero total current, then the ratio

$$-\left(\frac{\nabla\phi}{\nabla\xi}\right) \Bigg|_{J_{\text{Total}} = 0} = L_{21}/\sigma = C_{21}$$

gives the voltage coupling coefficient (C_{21}) in units of volts per unit of primary potential. If, in addition, the conductivity is measured (or the current is measured under the conditions of zero potential), then the current coupling coefficient (L_{21}) can be determined. For fluid flow, the primary potential is pressure and the coefficient $C_{21} = -(\nabla\phi / \nabla P)|_{J_{\text{Total}} = 0}$ is known as the streaming potential coefficient. The alternative measurement $L_{21} = -(J_{\text{Total}} / \nabla P)|_{\nabla\phi = 0}$ gives the streaming current coefficient. Because the measurement technique is easier, voltage coupling coefficients are more commonly reported in the literature and they will be used in the modeling that follows.

For simple problems with analytic solutions, there are no particular advantages to using equation 7 compared to the use of pseudopotentials. However, for more complicated problems requiring the use of numerical techniques, the application of equation 7 is straightforward and the solution of the coupled problem (3) requires no more than the solution of another potential problem. The first step is to use an appropriate program to solve the primary potential problem (fluid flow, heat flow, etc.). The second step consists of using the primary potential solution along with a model for the cross-coupling coefficients to calculate the sources for the electric problem from equation 7. The final step makes use of the current

sources along with an electrical model to determine the resultant electric potentials.

This procedure has been implemented with a 2-D transmission surface algorithm for the solution of potential problems.

NUMERICAL MODELING

The transmission surface algorithm for the DC potential problem is given in Madden (1971). A brief review is given here starting with the general potential flow equations,

$$\Gamma = -L \nabla \zeta , \quad (8)$$

and
$$\nabla \cdot \Gamma = S \quad (9)$$

where Γ is the flux, ζ is the potential, S is the source and L is the "conductivity". When L is independent of y (strike direction), equations 8 and 9 can be Fourier (cosine) transformed in the y -direction giving

$$-L(x,z) \frac{\partial \zeta (x, \lambda, z)}{\partial x} = \Gamma_x(x, \lambda, z) \quad (10)$$

$$-L(x,z) \frac{\partial \zeta (x, \lambda, z)}{\partial z} = \Gamma_z(x, \lambda, z) \quad (11)$$

$$\frac{\partial \Gamma_x}{\partial x} + \frac{\partial \Gamma_z}{\partial z} + \lambda^2 L \zeta = S(x, \lambda, z) \quad (12)$$

The flux and the potential are in general 3 dimensional, depending on the nature of the source. Equations 10, 11, and 12 can be approximated by lumped-element rectangular network (Figure 2) and the difference equation at a node is

$$\begin{aligned} & Y_x(i,j-1)[\zeta(i,j-1) - \zeta(i,j)] + Y_x(i,j)[\zeta(i,j+1) - \zeta(i,j)] \\ & + Y_z(i-1,j)[\zeta(i-1,j) - \zeta(i,j)] + Y_z(i,j)[\zeta(i+1,j) - \zeta(i,j)] \\ & + Y(i,j)\zeta(i,j) = S(i,j) \Delta x \Delta z \end{aligned} \quad (13)$$

where
$$Y_x = L \Delta z / \Delta x \quad (14)$$

$$Y_z = L \Delta x / \Delta z \quad (15)$$

$$Y = \lambda^2 \Delta x \Delta z, \quad (16)$$

$$i = 1 \dots n \quad ,$$

and $j = 1 \dots m \quad .$

The set of $n \cdot m$ node equations can be reorganized into the matrix equation

$$C \zeta = S \quad (17)$$

where $C =$ coefficient matrix [$n \cdot m \times n \cdot m$] ,

$\zeta =$ node potential vector ($n \cdot m$) ,

and $S =$ node source vector ($n \cdot m$) .

One method of solution of equation 17 is outlined by Swift (1967), who also provided the code (Swift, personal comm.). The final solution in x, y, z space is obtained by an inverse Fourier transform of a suite of $\zeta(\lambda)$ solutions.

The solution of the coupled problem requires three models for the physical properties, the primary flow resistivity (L_{11}^{-1}), the voltage cross-coupling coefficients ($C_{21} = \rho L_{21}$) and the electrical resistivity (ρ). For each λ value, the primary flow potentials (ζ) are computed for the primary model given a source distribution. From the divergence equation 7, the electrical source terms are calculated at each node. In the lumped circuit, the divergence equation 13 is used with L replaced by the cross coupling coefficients L_{21} . In the last step, the electrical source terms calculated in the previous step are used with the resistivity model to determine the electrical

potentials (ϕ).

The solution of these problems is formulated in equation 17 in terms of a flow source which is commonly taken as a point source. Finite-length line source distributions can be easily computed by simple convolution of the point source solution along the source line. In other applications, a specified potential distribution (Dirichlet boundary condition) rather than flow source distributions may be desirable. A simple procedure for accomplishing this, without disturbing the formal solution of equation 17, is outlined in Killpack and Hohmann (1979).

MODEL RESULTS

The results of the model calculation are normalized to dimensionless primary potentials (ζ_n) and dimensionless electric potentials (V_n) defined below

$$\zeta_n = \frac{(L_{11}a)}{I} \quad , \quad (18)$$

and

$$V_n = \frac{\phi}{C_{21}} \frac{(L_{11}a)}{I_\zeta} = \frac{\phi}{C_{21}} \frac{(\zeta_n)}{\zeta} \quad , \quad (19)$$

where a = size scale, length dimension of one model unit
 and I_ζ = source for primary flow, in units of $T_1 \times \text{area}$.
 The true potentials (ζ, ϕ) can be obtained by multiplication by the appropriate factor, taking care to use a consistent set of units. One result of modeling with the voltage-coupling coefficient (C_{21}) is that the induced current sources are inversely proportional to the resistivity ($L_{21} = C_{21}/\rho$). Since the voltage is proportional to the current-resistivity product, the resultant model voltages depend only on resistivity ratios. That is, the same potentials will result for all models that differ only by a multiplicative factor in all the model resistivities.

In the models that follow the distance scales are given in units of a and the model parameters are given as resistivities and voltage coupling coefficients where ρ = electrical resistivity, ρ_t = thermal resistivity, ρ_p = hydraulic resistivity or impermeability and c = voltage coupling coefficient. The parameter units, which are unspecified in most of the models, can be any consistent set or,

alternatively, they can be considered dimensionless. If the value of a parameter is unspecified, its value is unity.

Surface boundary conditions for the primary problem require careful consideration as the form of the flow near the air-earth interface can have a profound effect on the resultant electric potentials. For temperature problems the appropriate boundary condition is a constant temperature, which is taken as zero. With this boundary condition there is a normal flux of heat at the surface and there will be induced electrical sources here, if the surface medium has a non-zero coupling coefficient.

While it is correct that the excess pressure is zero from the water table up to the surface, uncritical use of the zero surface pressure boundary condition in potential-flow problems often results in a non-zero normal gradient and therefore a fluid flow at the air-earth interface. As was noted in Sill and Johng (1979), it is much more important to model the flow geometry which is predominantly horizontal near the surface or the water table. Horizontal fluid flow at the surface in a potential-flow problem requires a zero vertical gradient of the pressure. In the models, zero vertical gradients are produced by giving the air a vanishingly small hydraulic permeability. A water table below the surface can be modeled with a thin, very low-permeability layer overlain by more permeable near-surface material. In effect the modeled flow is confined by impermeable layers rather than having the flow deviated by variations in the height of the water table.

Figures 3 and 4 show the voltage in a vertical (x, z plane) plane, generated by point sources of pressure and temperature in a homogeneous half space. As discussed above, the surface boundary condition for pressure problems is zero normal gradient of pressure and for the thermal problem it is zero temperature at the surface. Comparing these figures we see that the pressure source produces an electrical anomaly at the surface while the temperature source has an equipotential coincident with the surface. In the case of the pressure source, the surface fluid flow is parallel to the air-earth interface and the only induced electrical source is at the pressure source where $\nabla^2 P \neq 0$. For the temperature problem there are induced electrical sources at the temperature source where $\nabla^2 T \neq 0$ and at the surface where there is a normal flux of heat. On the surface, the induced electrical sources at the interface exactly cancel the effects of the source at depth.

These two cases can be solved analytically and they both have zero total current, i.e., the electrical current exactly cancels the convection current. The primary potentials and flows have the same geometry as the electrical potentials and currents. The analytical solutions can also be used to check the model calculations. Comparisons of results show errors of a few percent for distances from the source greater than one unit, using a model discretization of one-quarter unit.

Both Nourbehecht (1963) and Fitterman (1978) state that there is no surface anomaly due to a point source of pressure in a homogeneous half space. The reason for this result is their use of the surface

boundary condition of zero pressure. In this case the desire to have the total potential equal to the electric potential has led to the use of an inappropriate boundary condition. As we have seen above, the appropriate boundary condition is zero normal gradient not zero pressure, in which case there is a surface anomaly. The models presented in Fitterman (1978, 1979) use the boundary condition of zero primary potential on the surface and as such they are appropriate only for thermal sources even though he proposed them as valid solutions for pressure-flow problems.

Figure 5 shows the effects of pressure source location with respect to a vertical boundary where there is a change in coupling parameters only. For curve 1, with the source to the left of the boundary, we see that the induced electrical sources at the vertical interface reduce the magnitude of the potential relative to that in a homogeneous half space (compare with Figure 3). The anomaly is, however, symmetric with respect to the source location. When the source is on the boundary (curve 2) the anomaly is reduced to one-half its value in a homogeneous half space. Curve 3 shows a sharp anomaly, centered at the contact due to the negative induced sources at the vertical boundary, where there is flow into the coupling medium.

Figure 6 illustrates how changes in the resistivity ratio attenuate or amplify the pressure-induced anomaly with no change in the form. Figure 7 shows that changes in the "impermeability" (ρ_p) across a vertical contact change both the amplitude and the form of the surface anomaly. A thermal model, similar to the pressure model of Figure 6 is shown in Figure 8. Here, with a homogeneous

resistivity structure ($\rho_1/\rho_2 = 1$), the surface anomaly has a symmetrical dipolar form. The positive peak is over the positive induced sources at the air-earth interface and the negative is to the right of the contact and is due to the $\nabla^2 T \neq 0$ source at $z = 1$. Changing the resistivity contrast amplifies the anomaly on the resistive side and reduces it on the conductive side. For a resistive ratio of ten the asymmetry is so pronounced that the dipolar form is almost obliterated. Figure 9 shows the effects of an overburden on the vertical contact model. Even for a homogeneous resistivity the overburden produces an asymmetric dipolar form. The reduction of the positive peak is due to the induced sources at the horizontal contact being at a greater depth. Changing the overburden resistivity amplifies or attenuates the form.

Changes in the quarter-space resistivities (Figure 10) in the overburden model also produce profound effects. If the coupling medium has a resistivity less than the other quarter-space, the anomalies are essentially monopolar and asymmetric. Changes in the primary flow resistivities can also produce significant effects on the form of the anomaly (Figure 11). Here the anomalies range from monopolar to dipolar as the thermal resistivity of the quarter-spaces is varied.

Although the basic pressure anomaly for the quarter space model is monopolar (Figures 5, 6 and 7), a dipolar anomaly can be produced if the overburden has a very large permeability so that there is vertical flow across horizontal boundaries (Figure 12). This flow pattern is then similar to the temperature flow problem in that

significant positive electrical sources are induced at the overburden interface. However, changes in the quarter-space electrical resistivities can alter this dipolar form.

Monopolar temperature anomalies can be produced with horizontal boundaries (layer over a half space) as in Figure 13. The sign of the anomaly can be changed by making the overburden the stronger cross-coupling medium.

The interactions of point sources with two vertical interfaces are shown in the dike models of Figures 14 and 15. With a point source located in the center of the dike (model 1, Figures 14 and 15), the surface anomaly is symmetrical because the flows and the induced sources are symmetrical with respect to the center of the dike. For the temperature source, the anomaly is positive over the dike, due to the positive induced sources at the air-earth interface, with negative wings off to the sides. The negative portions are due to the larger effect of the divergence of the heat flow from the point source when viewed from the sides. Moving the point temperature source to the left side of the dike (model 2, Figure 14) enhances the negative effect from the divergence of heat flow and produces a dipolar form. A dipolar form is also produced by a sequential increase in the coupling (model 3, Figure 14).

Reversing the contrast in the thermal model 1 of Figure 14 so that $c = 0$ in the dike and $c = 1$ exterior causes a reversal in signs of the anomaly (not shown). The same reversal in contrast in the pressure model, Figure 15-model 3, causes no change in the sign but there is a change in the form and a large change in the magnitude. In

this case there are only negative induced sources on the planes at $x = 0, 1$ due to the outward flow.

Moving the pressure source to the left side of the dike produces an asymmetric, negative anomaly (model 12, Figure 15) the broad negative to the left is due to the larger effect of the divergence at the source. As the observation point moves toward the right side the positive induced source on the plane at $x = 1$ rapidly cancels the effects of the negative electrical source at the point source of the divergence of the flow.

Consideration of the results from model 2, Figure 15 indicates that the combination of a positive pressure source at $x = 0$ and a negative source at $x = 1$, on either side of the dike, would produce a dipolar anomaly. In general, any relatively uniform flow across a dike would tend to produce a dipolar form.

Plan views ($z = 0$) of the contoured surface voltage are shown for models 1 of Figures 14 and 15 are shown in Figure 16. For a temperature source, Figure 16a, the positive part of the dipolar anomaly is elongated along strike (y direction) and for a pressure source, Figure 16b, the monopolar anomaly tends to be elongated perpendicular to strike.

FIELD EXAMPLE

The Monroe-Red Hill (Utah) geothermal system is an example of deep circulation along a fault zone that has been relatively well studied (Mase et al., 1978). A limited SP survey over the Red Hill area (Figure 17) showed a modest anomaly of dipolar form that correlated reasonably well with certain features of the electrical resistivity anomaly as delineated by dipole-dipole measurements. Figure 18 shows the physical properties model and the location of the thermal sources. The resistivity model is a generalization of models in Mase et al. (1978). The main features are a steeply dipping fault separating the volcanics on the east ($20\Omega\text{m}$) from the alluvium on the west. Away from the fault and near the surface the alluvium is moderately resistive ($25\text{-}50\Omega\text{m}$). Near the fault and at depth the alluvium is more conductive, probably due to the leakage of thermal waters and alteration. The thermal resistivity contrast between the volcanics and the alluvium is based on average values reported in Mase et al. (1978). The heat source distribution in the model represents the circulation of hot water up the fault and horizontal leakage into the alluvium. The temperature distribution from these sources is shown in Figure 18b; also shown are the observed temperatures at 25 m increments for four drillholes along the profile (Mase et al., 1978). The drillhole temperatures have been corrected for the mean temperature and the thermal gradient ($15^\circ\text{C}/\text{km}$) which are not represented in the model calculations. The calculated and observed temperatures and vertical heat fluxes are in reasonable agreement.

considering the coarseness of the mesh (25 m) and the fact that several of the observed heat fluxes are based on gradient data at depths less than 10 m. The total heat input into the model is .36MW, which is much less than the total conductive heat loss (1.5MW) from Red Hill. However, the thermal anomaly at Red Hill is elongated along the direction of the fault. For a 400 m swath normal to the fault (about the width of the SP anomaly) the total conductive heat loss is about .5MW, which is only slightly greater than the heat input to the model. A comparison of the observed and calculated SP anomalies are shown in Figure 19. The comparison is reasonably good although it should be noted that the observed anomaly is not exactly symmetrical about the centerline. The cross-coupling coefficients in the model are all larger than those typically reported in the literature, which seems to be a common problem (Fitterman and Corwin, 1981; Corwin et al., 1980). However, it should be noted that most samples reported on in the past were relatively unaltered material and the effects of elevated temperatures on the cross-coupling coefficients are not well known. Increasing temperatures should increase the current cross-coupling parameter through the increase in the diffusion constant, but for the voltage cross-coupling parameter this will be somewhat offset by the increase in conductivity, since $C = L/\sigma$.

Summary

An alternative method for modeling SP based on induced current sources due to primary flows has been presented. The method has been implemented using a transmission surface algorithm that provides modeling capabilities for three-dimensional distributions of sources and two-dimensional structures.

The model results presented demonstrate the basic forms of the induced SP response and how the anomalies are changed in form and amplitude by changes in the model parameters.

A field example demonstrates the joint modeling of thermal and SP data at Red Hill Hot Spring, Utah. Although the derived cross-coupling coefficients might be considered large, the modeling technique provides a method for testing the constraints on the physical parameters.

ACKNOWLEDGEMENTS

This work was funded by contract DE-AC07-80ID12079 from the Department of Energy, Division of Geothermal Energy. Additional thanks go to C. M. Swift Jr. for supplying the coding for the transmission surface algorithm and for his encouragement.

REFERENCES

- Bogoslovsky, V. V., and Ogilvy, A. A., 1973, Deformations of natural electric fields near drainage structures: *Geophys. Prosp.*, v. 21, no. 4, p. 716-723.
- Corwin, R. F., DeMouilly, G. T., and Harding, R. S. Jr, 1980, Interpretation of self-potential survey results from the East Mesa geothermal field, California: Preprint, paper submitted to *J. Geophys. Res.*
- Corwin, R. F., and Hoover, D. B., 1979, The Self-potential method in geothermal exploration: *Geophysics*, v. 44, p. 226-245.
- Corwin, R. F., and Morrison, H. F., 1977, Self-potential variations preceding earthquakes in central California: *Geophys. Res. Lett.*, v. 4, p. 171.
- de Witte, L., 1948, A new method of interpretation of self potential data: *Geophysics*, v. 13, no. 4, p. 600-608.
- Fitterman, D. V., 1978, Electrokinetic and magnetic anomalies associated with dilatent regions in a layered earth: *J. Geophys. Res.*, v. 83, p. 5923.
- Fitterman, D. V., 1979, Calculations of self-potential anomalies near vertical contacts: *Geophysics*, v. 44, p. 195-205.

Fitterman, D. V., and Corwin, R. F., 1981, Inversion of self-potential data from the Cerro Prieto geothermal field, Mexico: Preprint, paper submitted to Geophysics.

Killpack, T. J., and Hohmann, G. W., 1979, Interactive dipole-dipole resistivity and IP modeling of arbitrary two-dimensional structures: DOE/DGE Report, contract EG-78-C-07-1701, Earth Science Laboratory, University of Utah Research Institute.

Madden, T. R., 1971, The resolving power of geoelectric measurements for delineating resistive zones within the crust, in The structure and physical properties of the earth's crust, ed T. G. Heacock: AGU Monograph 14, American Geophysical Union, p. 95.

Marshall, D. J., and Madden, T. R., 1959, Induced polarization, a study of its causes: Geophysics, v. 24, p. 790.

Mase, C. W., Chapman, D. S., and Ward, S. H., 1978, Geophysical study of the Monroe-Red Hill geothermal system: DOE/DGE topical report, contract EY-76-S-07-1601, University of Utah.

Meiser, P., 1962, A method for quantitative interpretation of self-potential measurements: Geophys. Prospect., v. 10, no. 2, p. 203-218.

Nourbehecht, B., 1963, Irreversible thermodynamic effects in inhomogeneous media and their application in certain geoelectric problems: Ph.D. thesis, Mass. Inst. of Tech., Cambridge.

- Ogilvy, A. A., Ayed, M. A., and Bogoslovsky, V. A., 1969, Geophysical studies of water leakages from reservoirs: *Geophys. Prosp.*, v. 22, no. 1, p. 36-62.
- Paul, K., 1965, Direct interpretation of self-potential anomalies caused by inclined sheets of infinite horizontal extensions: *Geophysics*, v. 30, no. 3, p. 418-423.
- Sill, W. R., and Johng, D. S., 1979, Self potential survey, Roosevelt Hot Springs, Utah: DOE/DGE topical report, contract DE-AC07-78ET28392, University of Utah.
- Swift, C. M. Jr., 1967, A magnetotelluric investigation of an electrical conductivity anomaly in the southwestern United States: Ph.D. thesis, Dept of Geology and Geophysics, Mass. Inst. of Tech., Cambridge.
- Yungul, Sulhi, H., 1950, Interpretation of spontaneous polarization anomalies caused by spheroidal orebodies: *Geophysics*, v. 15, no. 2, p. 237-246.

FIGURE CAPTIONS

- Figure 1. One-dimensional coupled flow. The discontinuity in convective current at $x = 0$, h produce planes of current sources giving rise to a linear potential increase in region 2.
- Figure 2. Lumped-element rectangular network
- Figure 3. Normalized voltage in the vertical plane ($y = 0$) for a point pressure source in a homogeneous half-space. The boundary condition at the surface is zero normal pressure gradient. The source of unit strength is at $x = 0$, $z = 1$ and distances are in units of a .
- Figure 4. Normalized voltage in the vertical plane ($y = 0$) for a point temperature source in a homogeneous half-space. The boundary condition at the surface is zero temperature. The source of unit strength is at $x = 0$, $z = 1$ and distances are in units of a .
- Figure 5. Surface voltage ($y = 0$, $z = 0$) for a point pressure source and a vertical contact, location of the source varies with respect to the contact.
- Figure 6. Surface voltage ($y = 0$, $z = 0$) for a point temperature source and a vertical contact, variations in the resistivity ratio across the contact.

- Figure 7. Surface voltage ($y = 0, z = 0$) for a point pressure source and a vertical contact. Variations in the permeability across the contact.
- Figure 8. Surface voltage ($y = 0, z = 0$) for a point temperature source and a vertical contact. Variations in the resistivity ratio across the contact.
- Figure 9. Surface voltage ($y = 0, z = 0$) for a point temperature source and a vertical contact - overburden model. Variations in the overburden resistivity.
- Figure 10. Surface voltage ($y = 0, z = 0$) for a point temperature source and a vertical contact-overburden model. Variations in the quarter-space resistivities.
- Figure 11. Surface voltage ($y = 0, z = 0$) for a point temperature source and a vertical contact-overburden model. Variations in the quarter-space thermal resistivities.
- Figure 12. Surface voltage ($y = 0, z = 0$) for a point pressure source and a vertical contact-overburden model. High permeability overburden and variations in the quarter-space resistivities.
- Figure 13. Surface voltage ($y = 0, z = 0$) for a point temperature source and an overburden model. Variations in the source location.

- Figure 14. Surface voltage ($y = 0, z = 0$) for a point temperature source and a dike. Variations in the source locations and coupling parameters.
- Figure 15. Surface voltage ($y = 0, z = 0$) for a point pressure source and a dike. Variations in the source locations and coupling parameters.
- Figure 16. Contours of surface voltage (x, y plane, $z = 0$) for point sources and a dike. (a) Point temperature source (model 1, Figure 14) (b) Point pressure source (model 1, Figure 15).
- Figure 17. Plan map of SP anomaly at Red Hill Hot Spring, Utah.
- Figure 18. (a) Physical properties used to model the data at Red Hill. (b) Comparison of the observed and calculated temperatures at Red Hill.
- Figure 19. Comparison of the observed and modeled SP anomaly at Red Hill. Model properties in Figure 15a.

1D FLOW

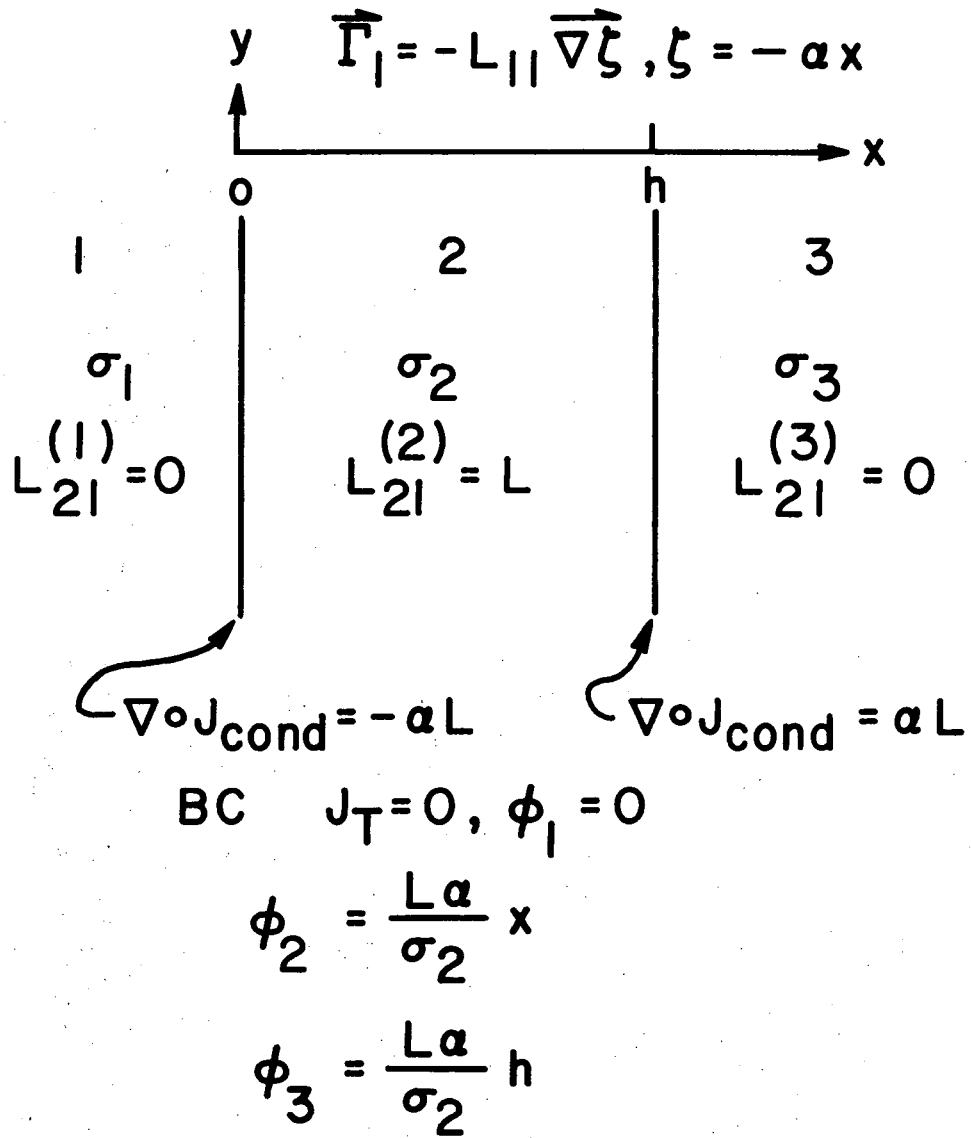


Figure 1

LUMPED CIRCUIT

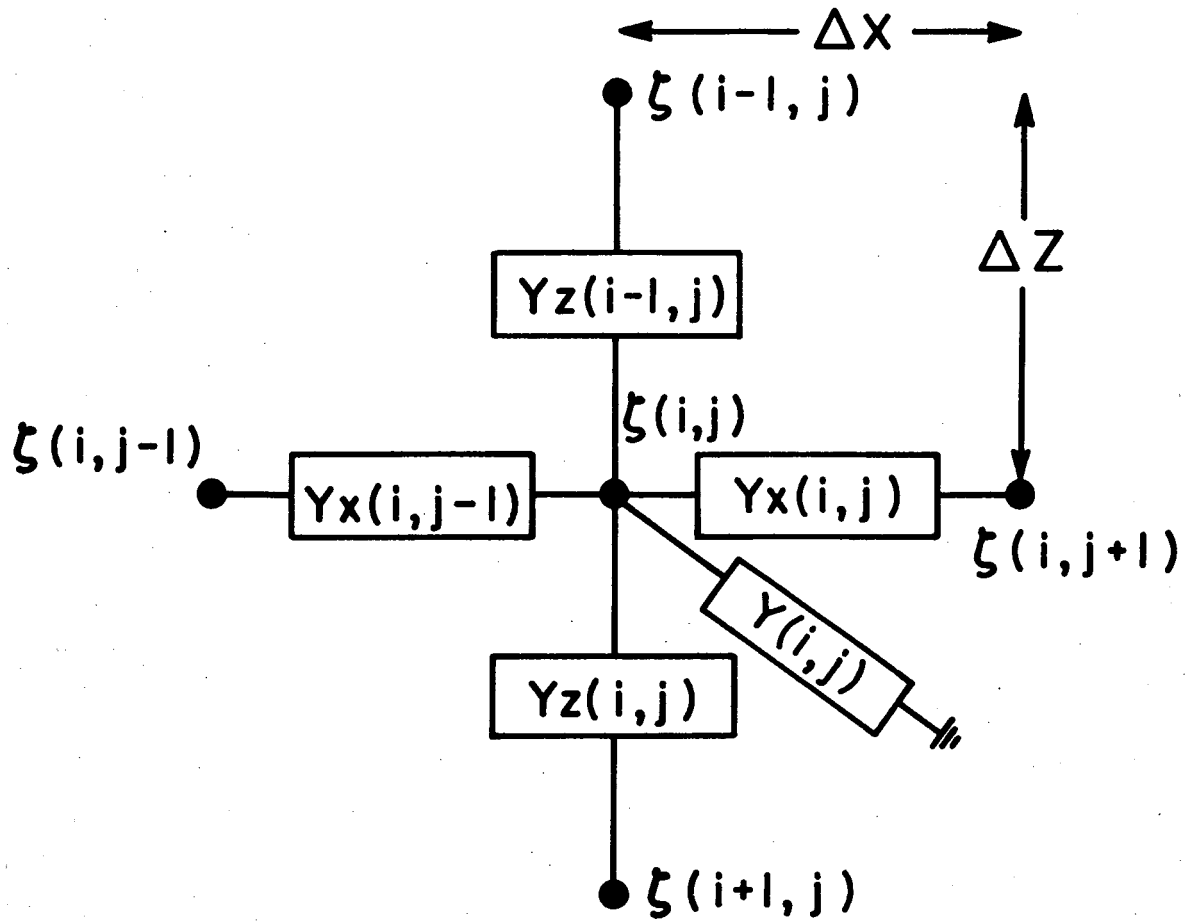


Figure 2

HOMOGENEOUS HALF-SPACE
POINT PRESSURE SOURCE
NORMALIZED VOLTAGE $-V_n$

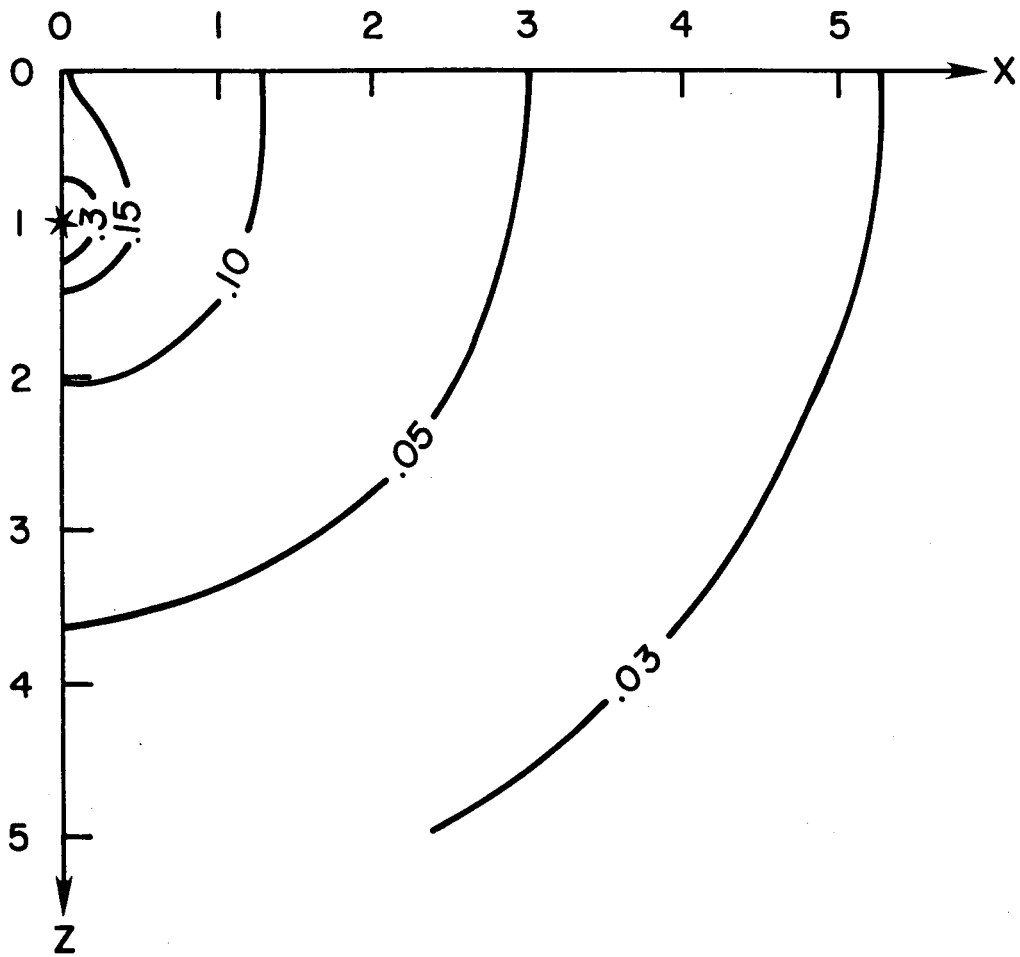


Figure 3

HOMOGENEOUS HALF-SPACE
POINT TEMPERATURE SOURCE
NORMALIZED VOLTAGE $-V_n$

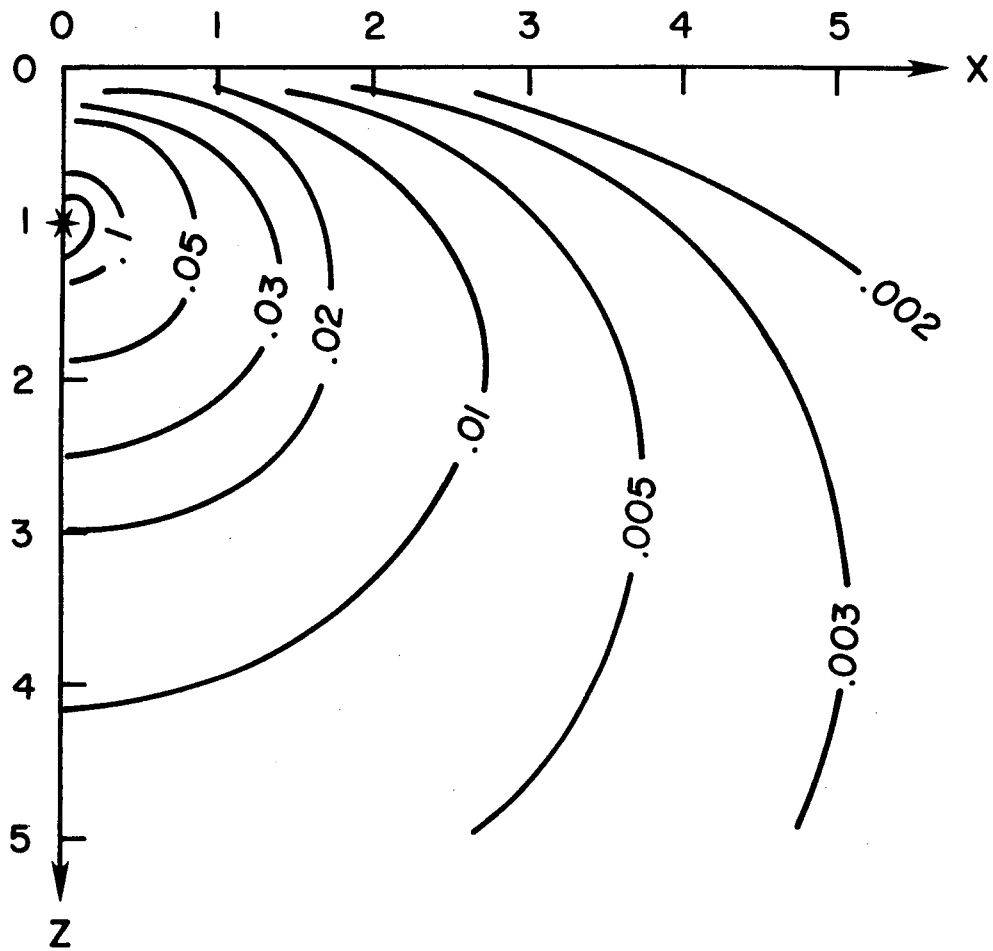


Figure 4

VERTICAL CONTACT
POINT PRESSURE SOURCE

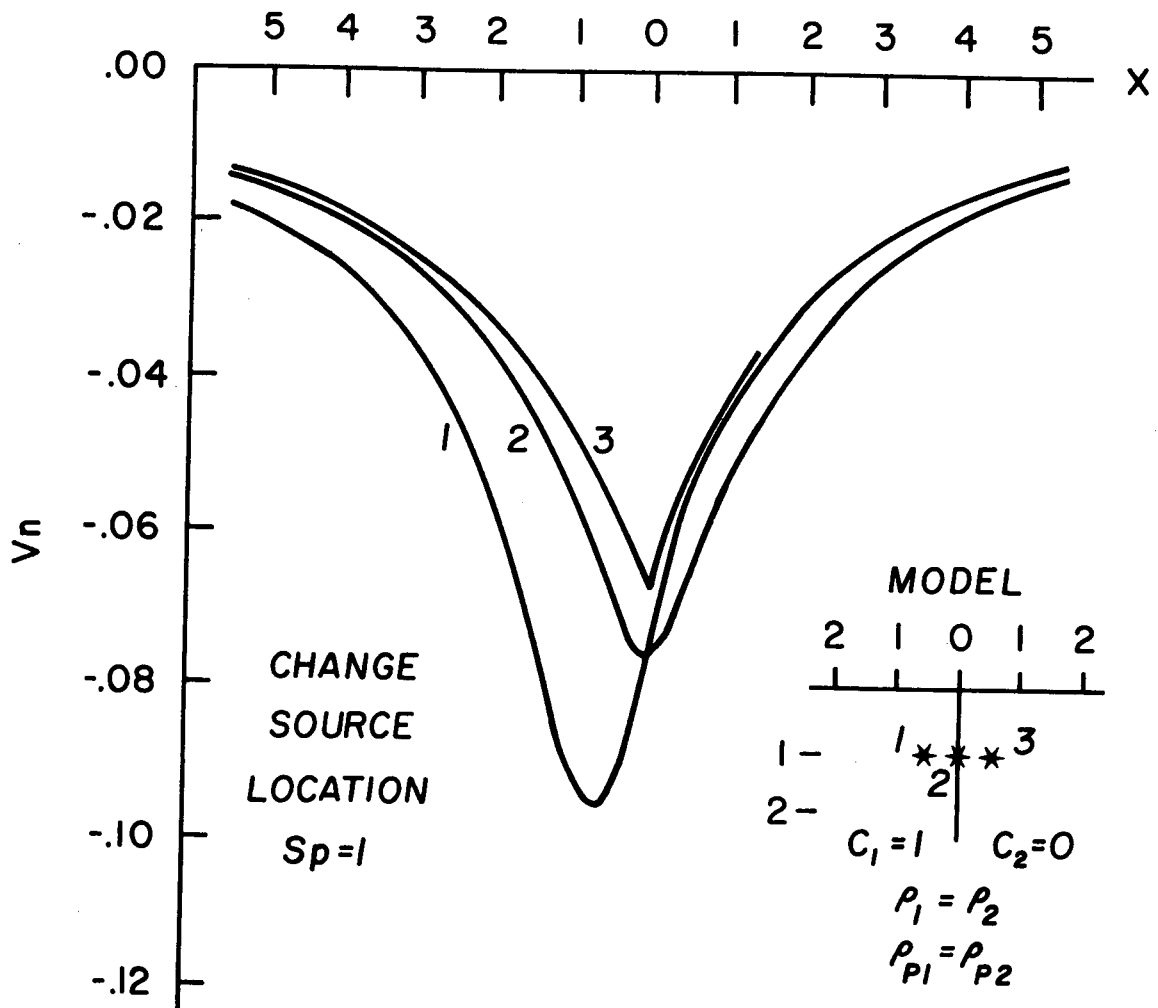


Figure 5

VERTICAL CONTACT
POINT PRESSURE SOURCE

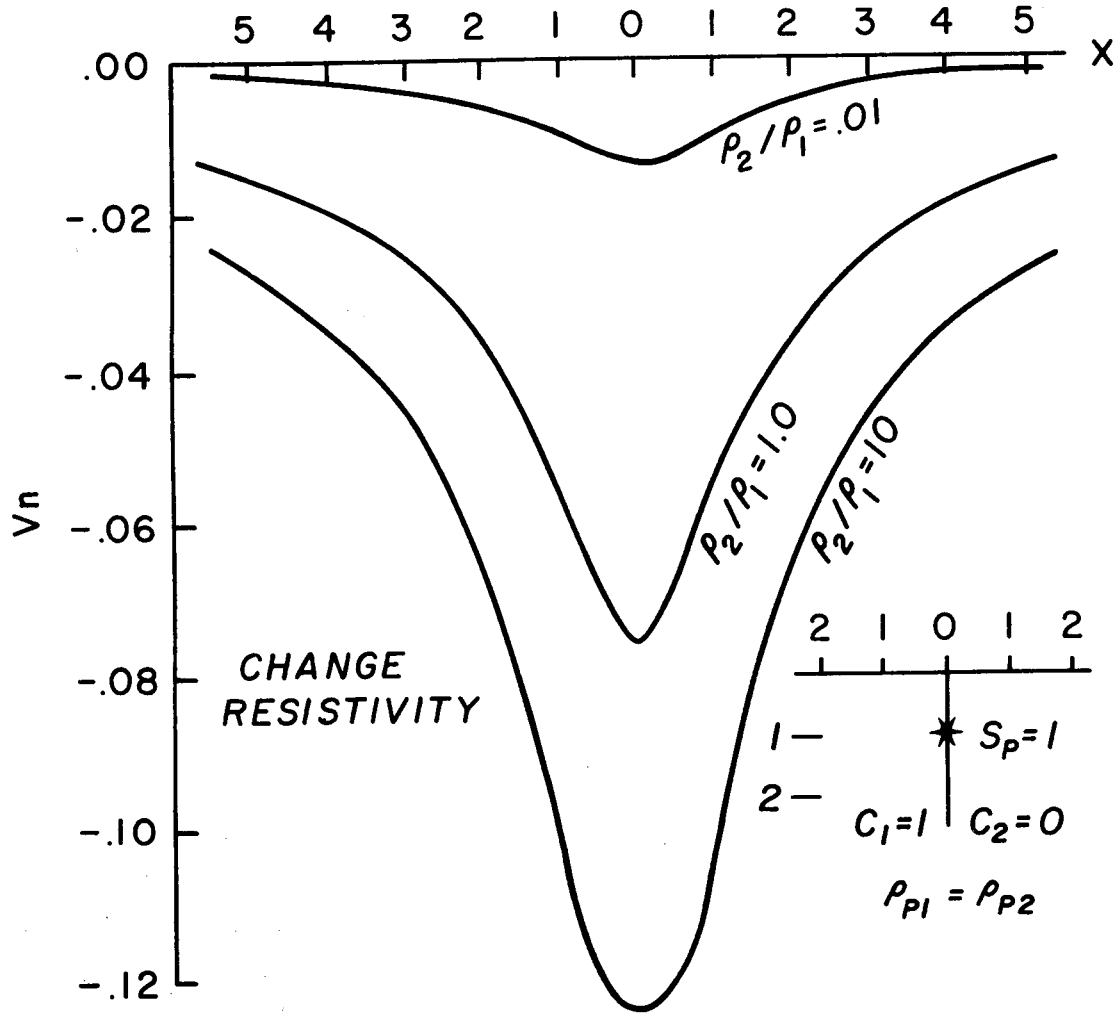


Figure 6

VERTICAL CONTACT
POINT PRESSURE SOURCE

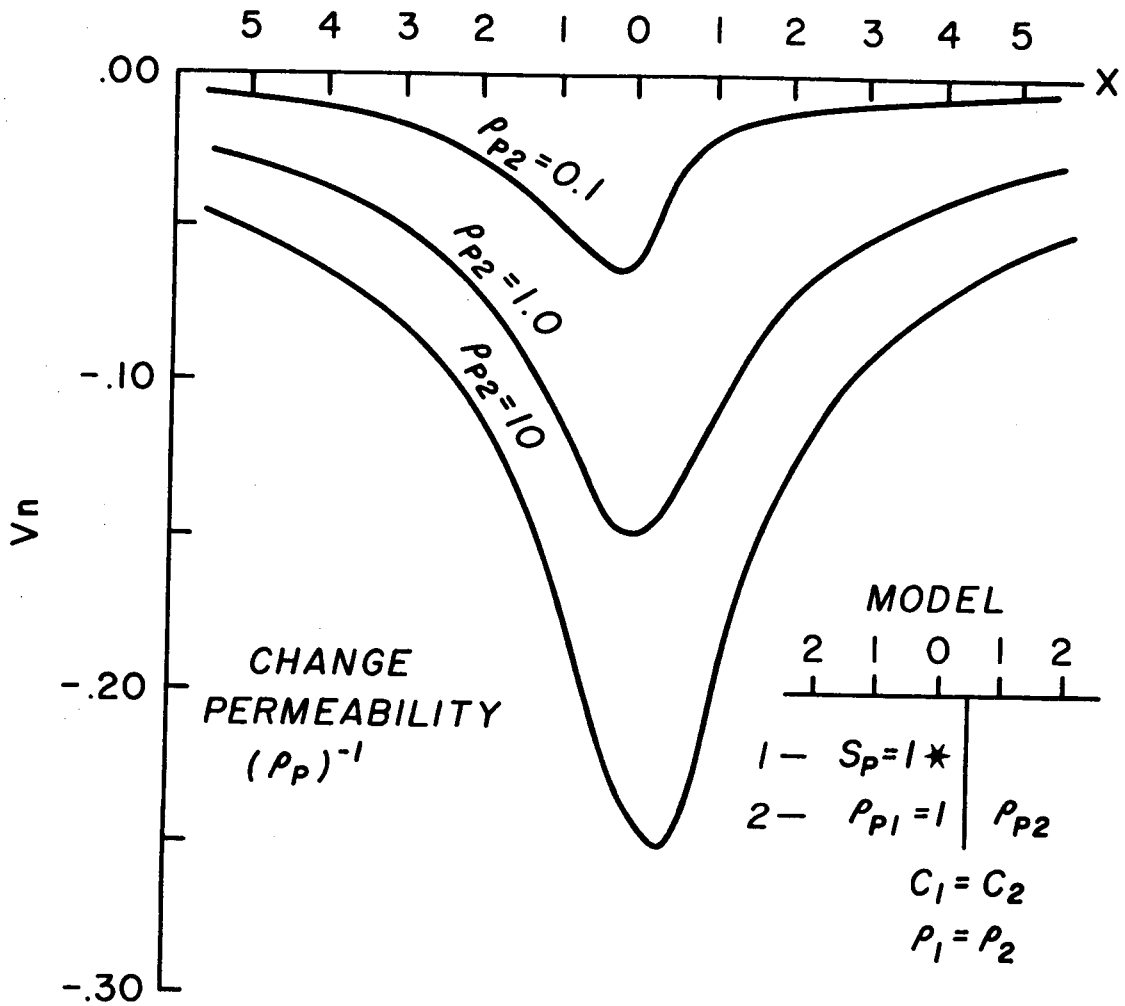


Figure 7

VERTICAL CONTACT POINT
TEMPERATURE SOURCE

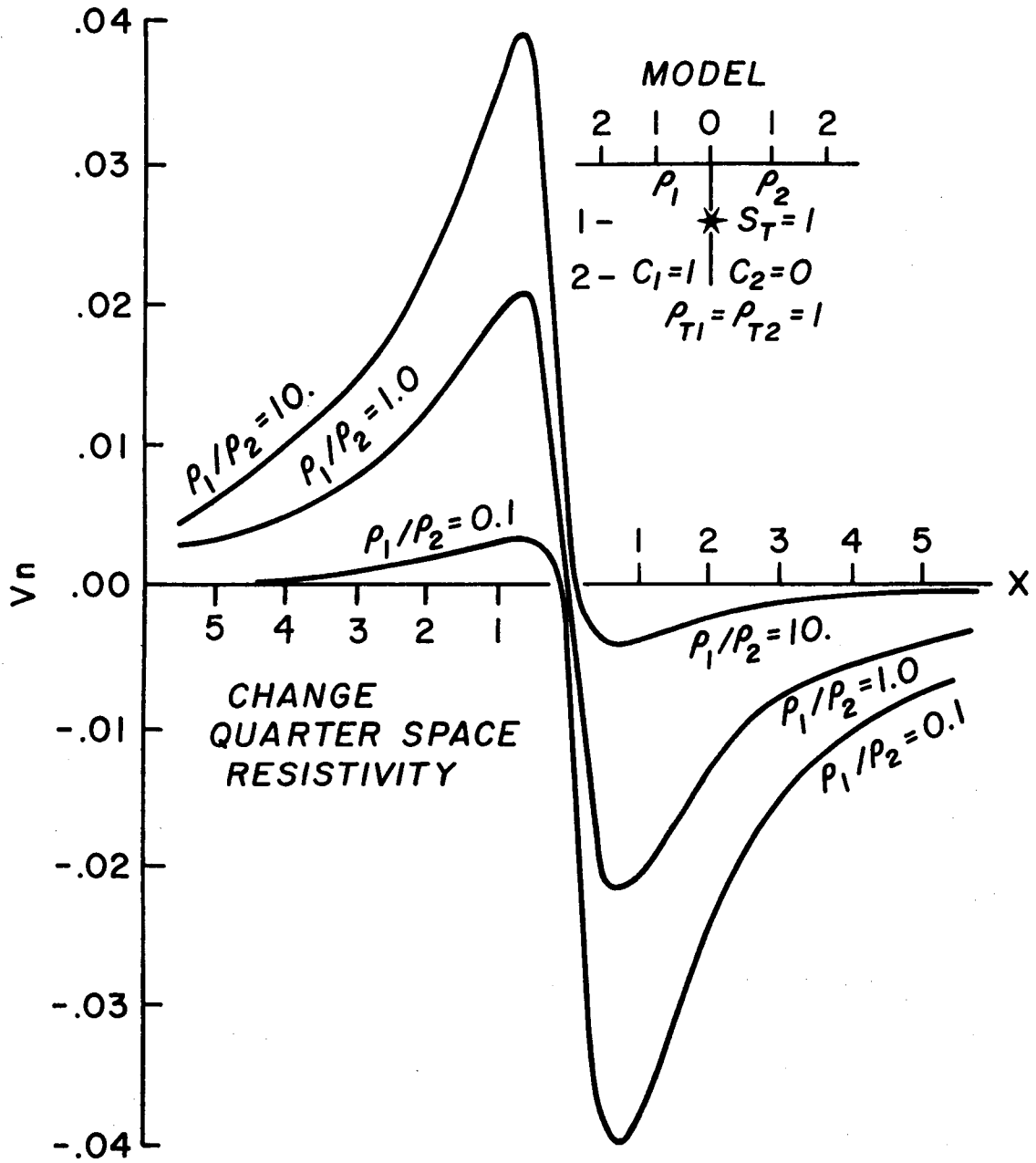


Figure 8

OVERBURDEN - VERTICAL CONTACT
POINT TEMPERATURE SOURCE

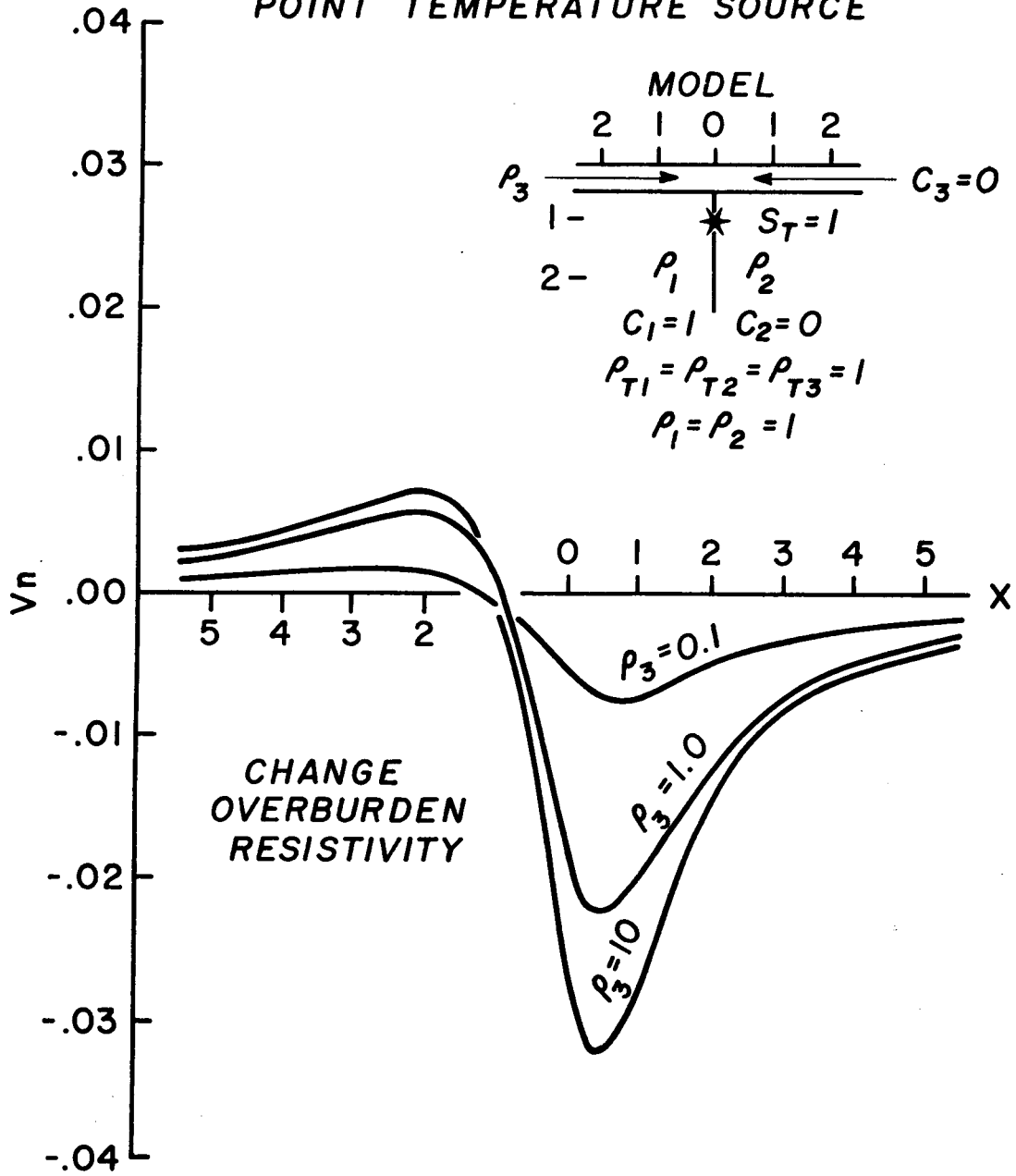


Figure 9

OVERBURDEN - VERTICAL CONTACT
POINT TEMPERATURE SOURCE

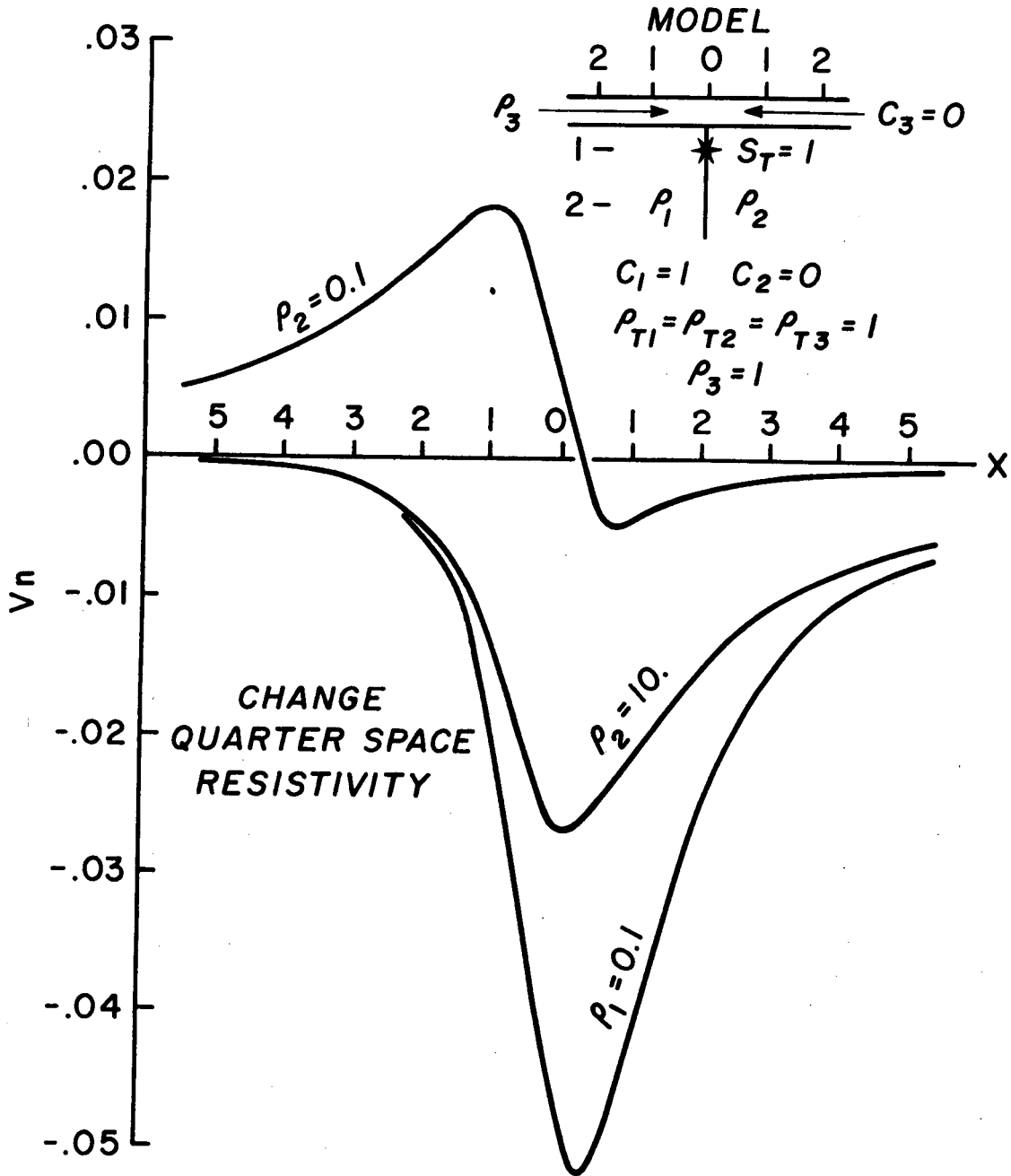


Figure 10

OVERBURDEN-VERTICAL CONTACT
POINT TEMPERATURE SOURCE

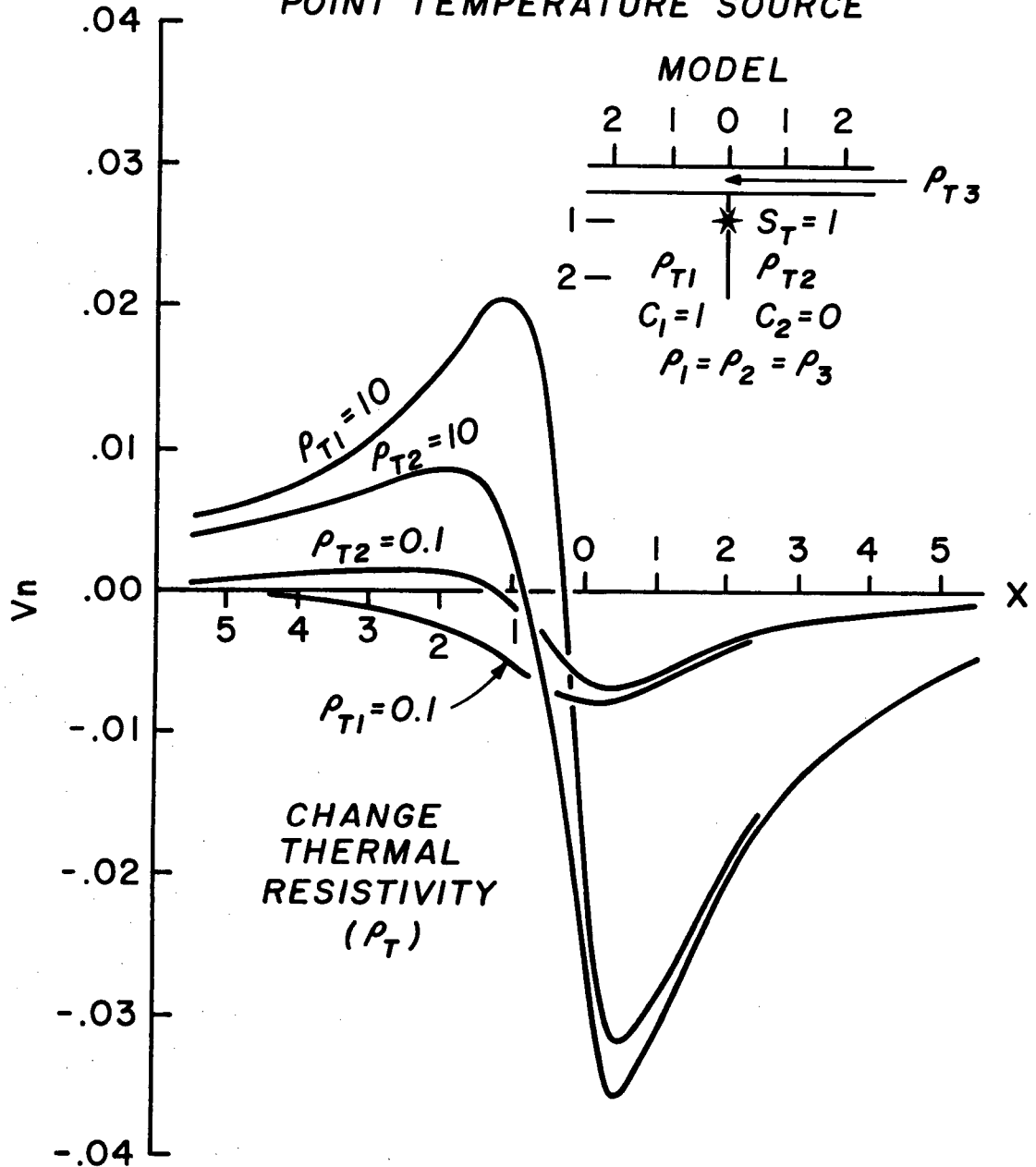


Figure 11

OVERBURDEN - VERTICAL CONTACT
POINT PRESSURE SOURCE

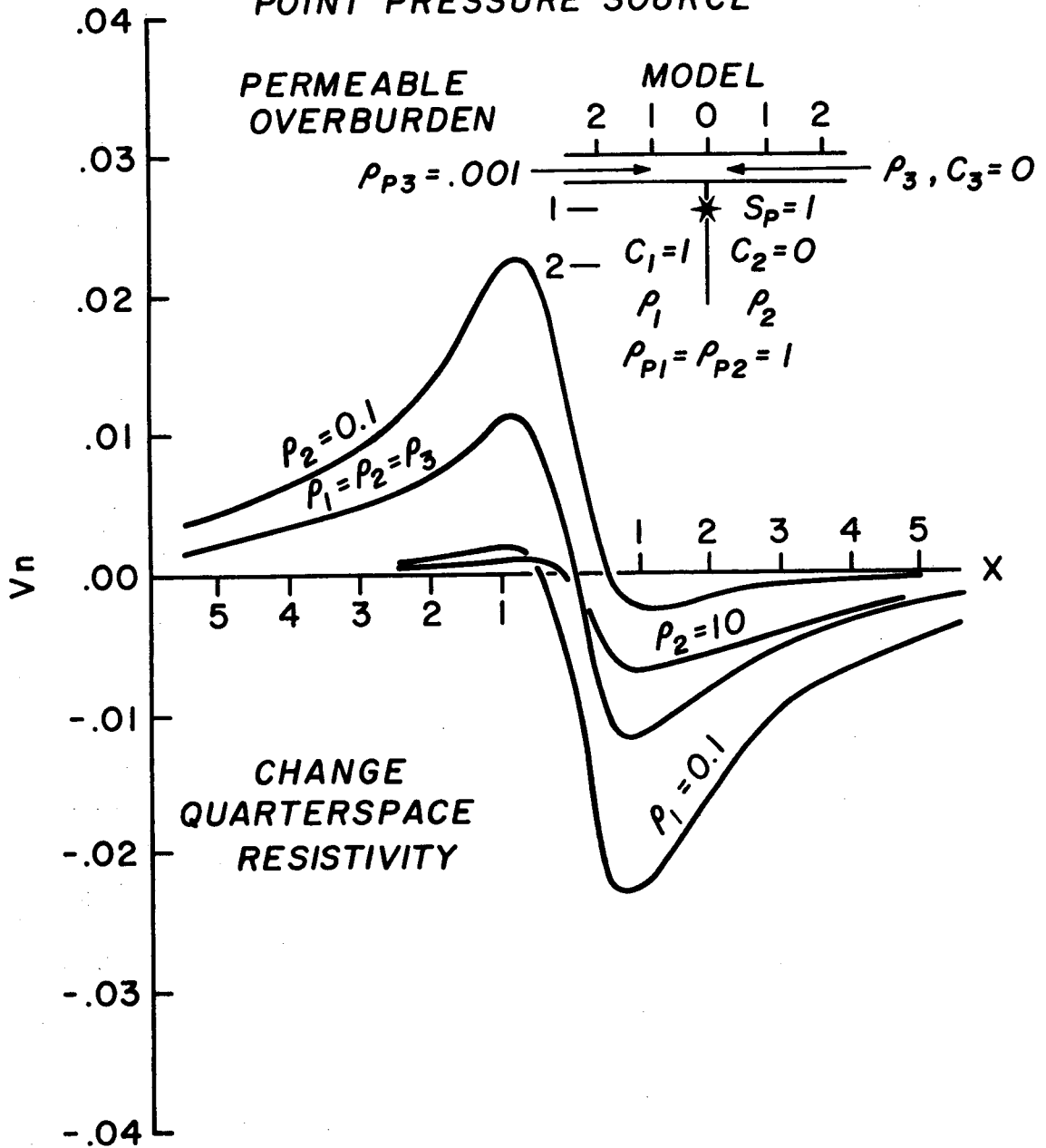


Figure 12

HORIZONTAL CONTACT
POINT TEMPERATURE SOURCE

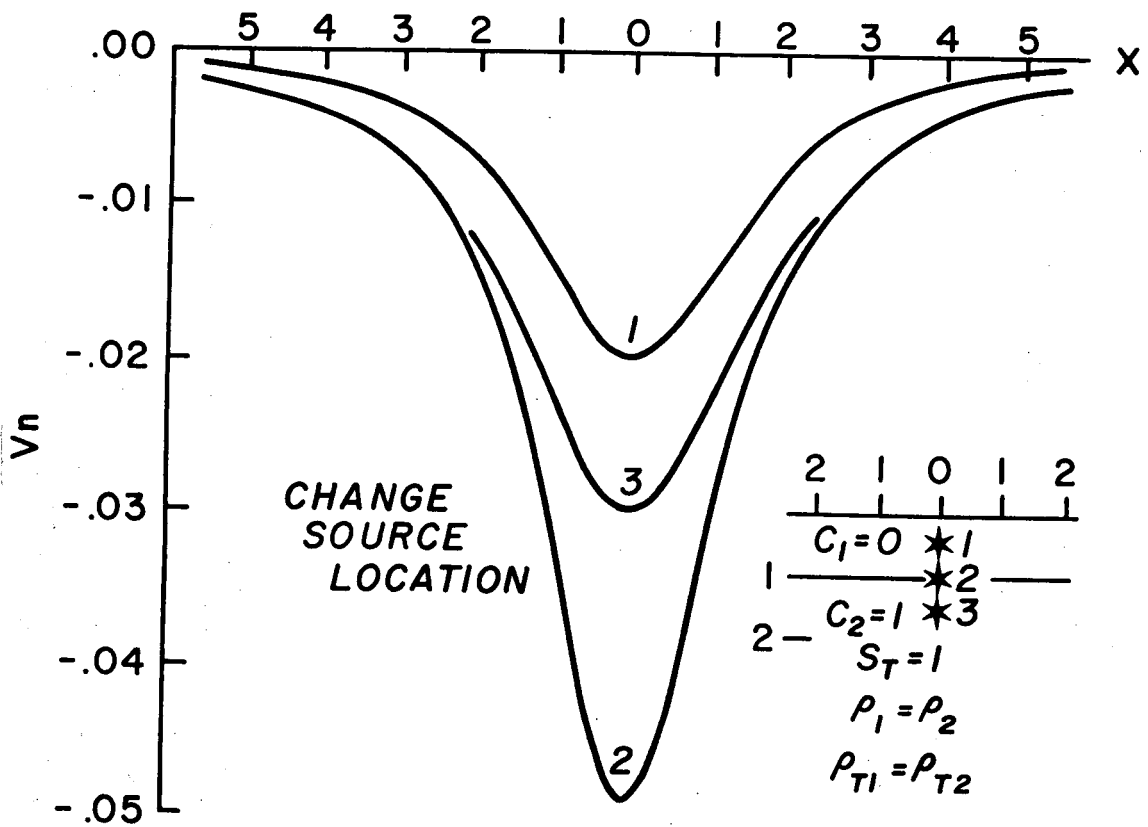


Figure 13

**VERTICAL DIKE
POINT TEMPERATURE SOURCE**

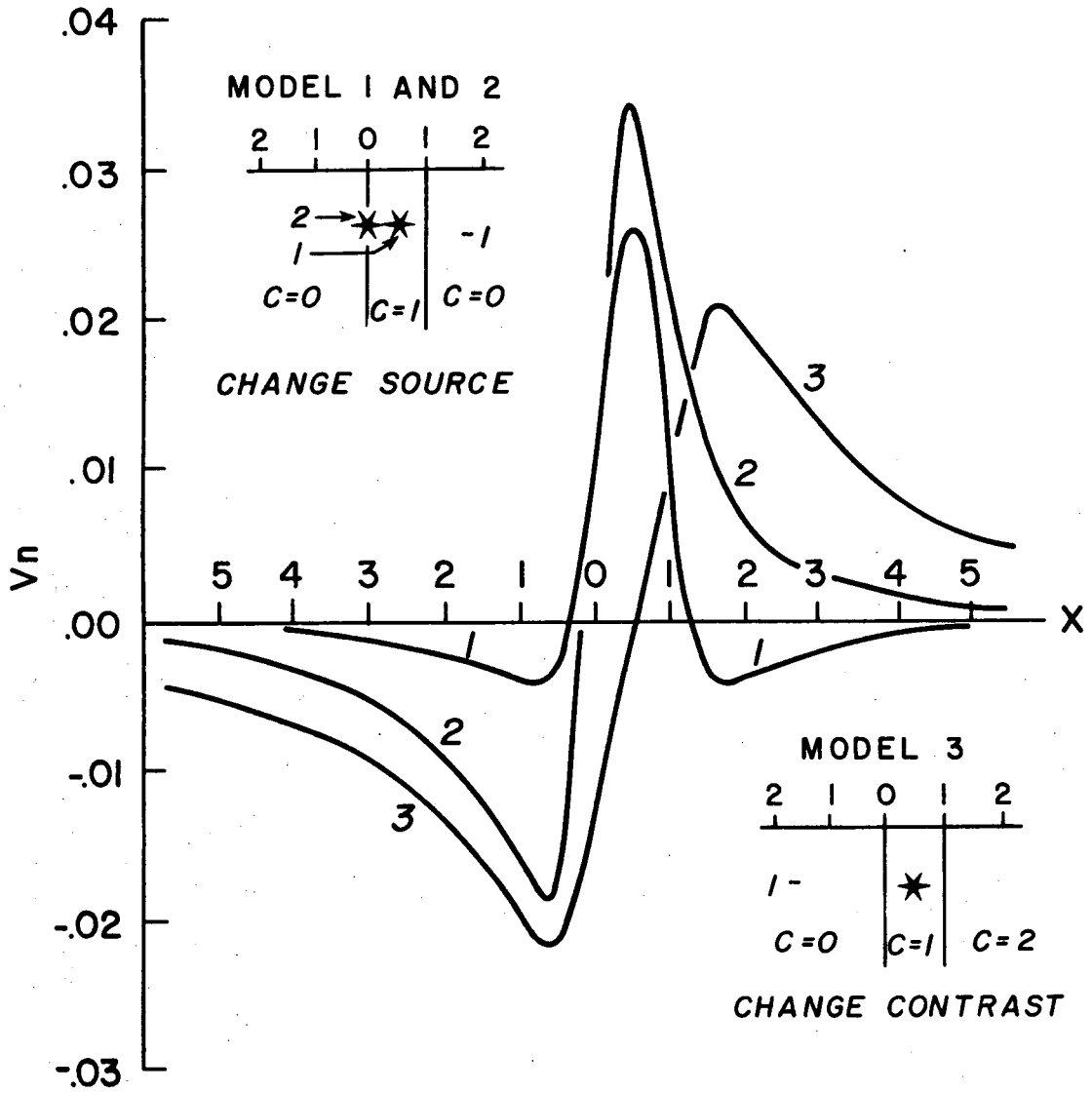
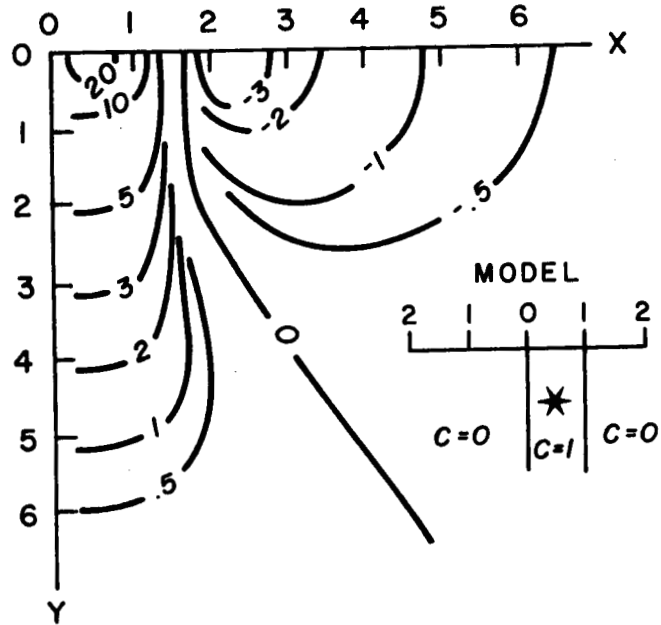


Figure 14

VERTICAL DIKE
VOLTAGE CONTOURS $V_n \times 10^3$
(a) TEMPERATURE SOURCE



(b) PRESSURE SOURCE

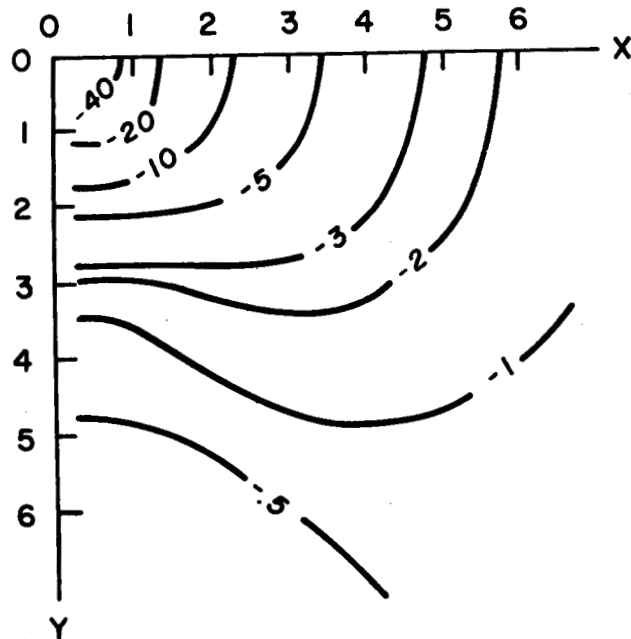
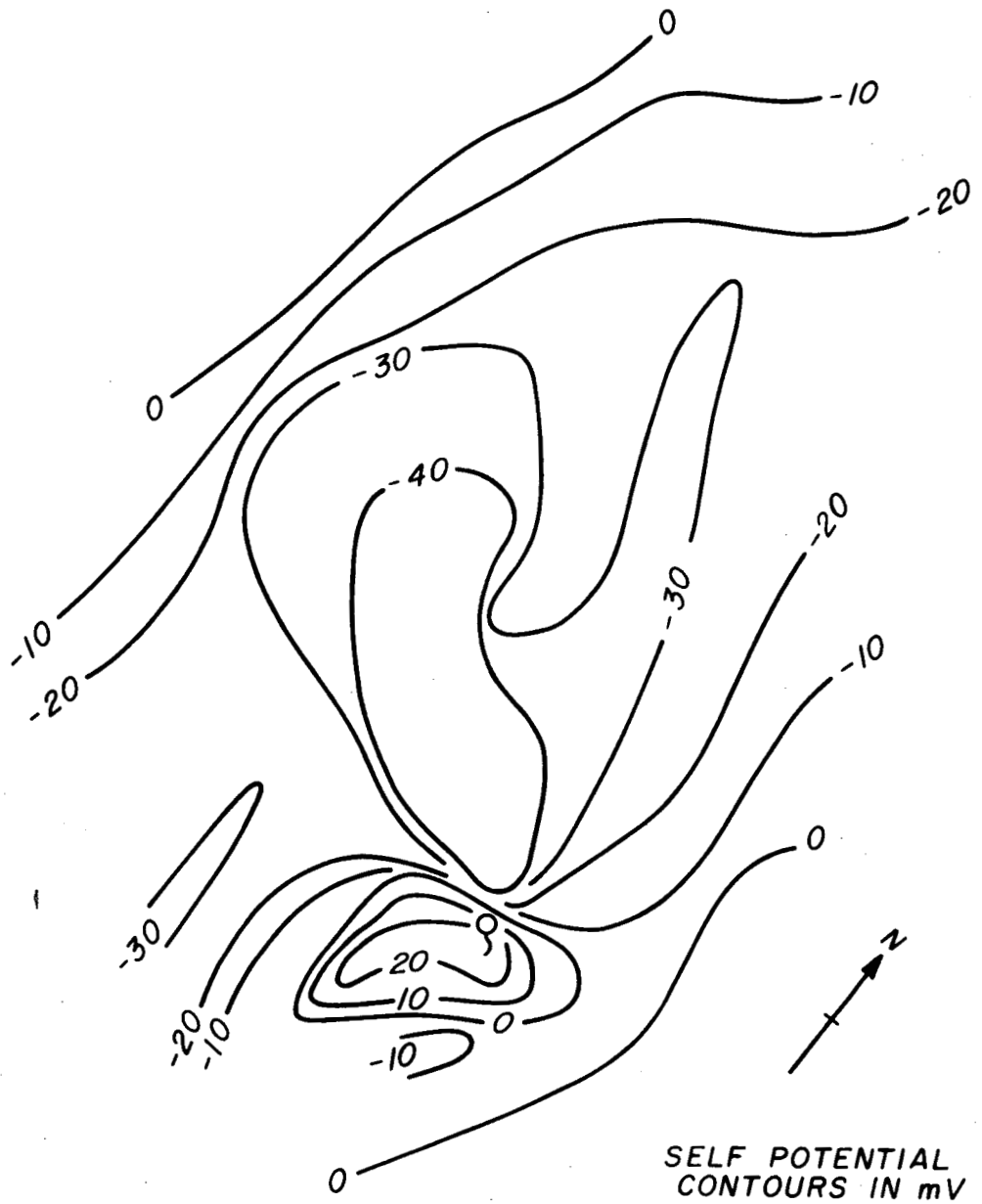


Figure 16



SELF POTENTIAL
CONTOURS IN mV

Red Hills Hot Springs
Monroe, Utah

SCALE
0 100 M

Figure 17

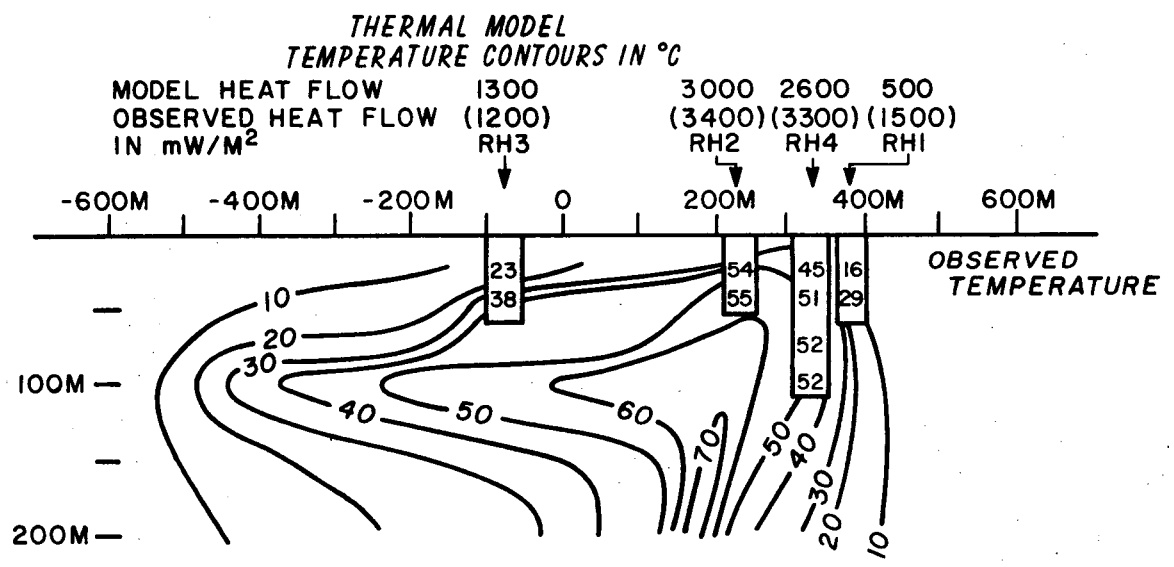
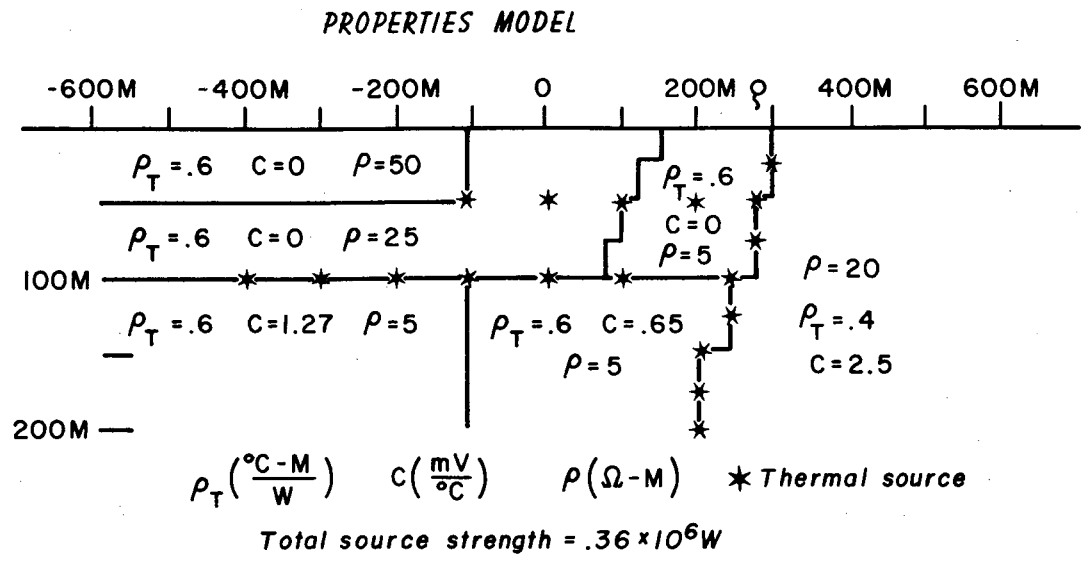


Figure 18

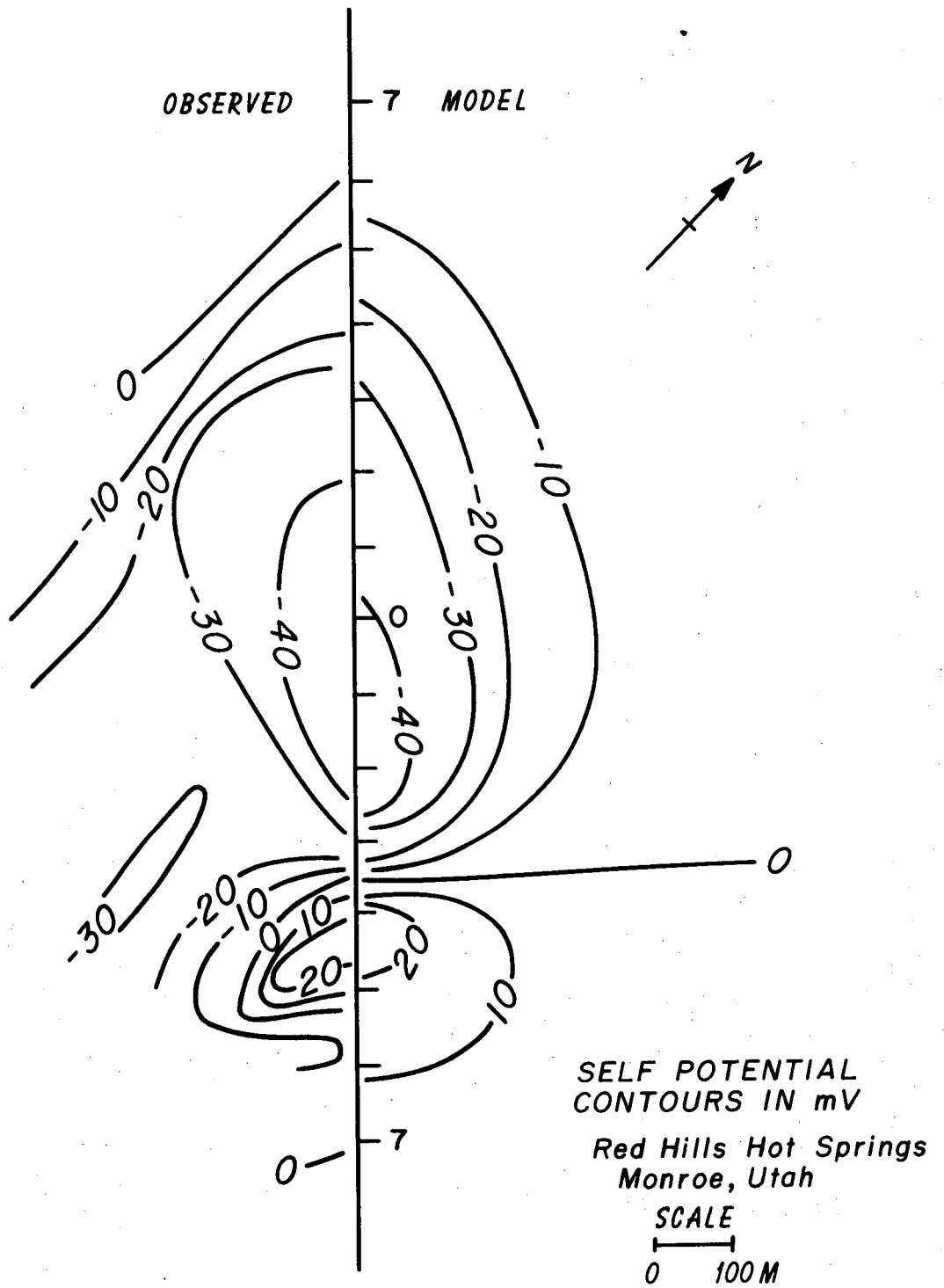


Figure 19